Monthly Notices
of the
ROYAL ASTRONOMICAL SOCIETY

MNRAS **469,** S598–S605 (2017)
Advance Access publication 2017 July 22

doi:10.1093/mnras/stx1873

Cometary coma dust size distribution from *in situ* IR spectra

G. Rinaldi,[1]★ V. Della Corte,[1,2]★ M. Fulle,[3]★ F. Capaccioni,[1] A. Rotundi,[1,2] S. L. Ivanovski,[1] D. Bockelée-Morvan,[4] G. Filacchione,[1] E. D'Aversa,[1] M. T. Capria,[1] G. P. Tozzi,[5] S. Erard,[4] C. Leyrat,[4] E. Palomba,[1] A. Longobardo,[1] M. Ciarniello,[1] F. Taylor,[6] S. Mottola[7] and M. Salatti[8]

[1]*Istituto di Astrofisica e Planetologia Spaziali, Istituto Nazionale di Astrofisica, I-00133 Rome, Italy*
[2]*Universita' degli Studi di Napoli Parthenope, Dip. di Scienze e Tecnologie, CDN IC4, I-80143 Naples, Italy*
[3]*INAF – Osservatorio Astronomico, Via Tiepolo 11, I-34143 Trieste Italy*
[4]*LESIA, Observatoire de Paris, LESIA/CNRS, UPMC, Universite Paris-Diderot, F-92195 Meudon, France*
[5]*INAF – Osservatorio Astrofisico di Arcetri, I-50125 Firenze, Italy*
[6]*Department of Physics, Oxford University, Oxford, OX1 3PU, UK*
[7]*Institute for Planetary Research, Deutsches Zentrum fur Luftund Raumfahrt (DLR), D-12489 Berlin, Germany*
[8]*ASI, Via del Politecnico snc, I-00133 Rome, Italy*

Accepted 2017 July 20. Received 2017 July 20; in original form 2017 April 20

ABSTRACT

Dust is the most abundant component in cometary comae. Here, we investigate the dust size distribution in 67P/Churyumov-Gerasimenko (67P/CG) using data from the *Rosetta* spacecraft that was in close proximity to the comet from 2014 August to 2016 September. The Visual, Infrared and Thermal Imaging Spectrometer (VIRTIS-M), spectral range of 0.25–5 μm, and the Grain Impact Analyser and Dust Accumulator (GIADA), both part of the *Rosetta* payload, together provide a powerful means to characterize the dust coma properties. On March 28, *Rosetta* performed a flyby close to the nucleus that allowed GIADA to detect a large amount of dust particles used to constraint the differential size distribution power-law index of -2.2 ± 0.3. In April 2015, VIRTIS-M observed the spectral radiance in the wavelength range of 1–5 μm. A simple radiative transfer model has been applied to simulate the VIRTIS-M radiances, thus allowing to infer the dust properties. We assumed an optically thin dust coma and spherical amorphous carbon particles in the size range between 0.1 to 1000 μm. We obtained the infrared data best fit with a differential dust size distribution power-law index of $-3.1^{+3}_{-0.1}$. This index matches the one determined using GIADA March 2015 data indicating that, before perihelion, the inner coma radiance is dominated by particles larger than 10 μm; and the dust coma did not change its properties during most of the 67P/CG inbound orbit.

Key words: comets: individual: 67P/Churyumov-Gerasimenko – methods: data analysis – methods: observational – space vehicles: instruments – techniques: imaging spectroscopy.

1 INTRODUCTION

Many published studies have proposed a variety of analytical forms for the size distribution n(a) of the dust ejected from the sunlit surface of a cometary nucleus, where n(a)da provides the number of particles with radius in the range of (a, a+da). Before the *Rosetta* mission, this quantity has never been properly measured, but inferred from ground-based and *in situ* data by means of geometrical models too simple to be realistic. For instance, in a comprehensive paper on particle detector results acquired during the Giotto flyby at comet 1P/Halley, McDonnell et al. (1987) converted the measured fluence into a dust size distribution at the nucleus surface, assuming a perfectly isotropic ejection and neglecting the contribution of large particles reflected by the solar radiation pressure. Fulle et al. (1995) have shown that this approach is unrealistic, and adversely affects the conversion of the measured fluence into the size distribution. McDonnell et al. (1987) give a typical mass distribution law of $n(m) \sim m^{-0.85}$, but the exponent apparently varies at various locations in Halley's coma. According to only two particles detected by the particle impact analyser, onboard Giotto, the fluence seems to flatten for particles smaller than 0.5 μm. McDonnell et al. (1987) converted the mass power law to a differential particle size distribution with a power law of −3.55. However, assuming an anisotropic dust ejection that makes, along the flyby trajectory, the

★ E-mail: giovanna.rinaldi@iaps.inaf.it (GR); vincenzo.dellacorte@iaps.inaf.it (VDC); fulle@oats.inaf.it (MF)

© 2017 The Authors
Published by Oxford University Press on behalf of the Royal Astronomical Society

Downloaded from https://academic.oup.com/mnras/article/469/Suppl_2/S598/4004761 by guest on 27 April 2021

flux of particles reflected by solar radiation pressure larger than that of particles directly coming from the nucleus; the same measured fluences provided a completely different size distribution at the nucleus surface, with a power index between −2.5 and −3.0 (Fulle et al. 2000).

Green et al. (2007) report the fluence measured by Stardust in the coma of comet 81P/Wild 2. They, too, converted the fluence into a size distribution, assuming a perfectly isotropic dust ejection and neglecting the important contribution of large particles reflected by the solar radiation pressure. They found the size distribution to be variable with an overall (averaged in time) power law exponent of −3.25. During the high-activity period, small grains dominated giving an exponent of −4.4. As in the 1P/Halley case, the dust size distribution at the nucleus surface probably had very different indexes. The smallest particles they detected were 3 μm in size.

Ground-based (or equivalent remote) observations need complex multiparametric models to infer the dust size distribution from the observed coma and tail images. *Spitzer* thermal infrared measurements provided excellent new data on the emission by solid species in cometary comae and in the ejecta generated by Deep Impact on 9P/Tempel 1 (Lisse et al. 2006, 2007). Different data analyses give conflicting results, reflecting the different assumptions made for the adopted coma models. According to some of the applied models, the ejecta plume of 9P/Tempel 1 had a particle size distribution with a power law of −3.8, while the quiescent coma follows a less steep power law. Jorda et al. (2007) present an analysis of the observations of the Deep Impact event. They consider spherical olivine particles (with a density of 3780 kg m^{-3}) and find that the slope of the differential dust size distribution is -3.1 ± 0.3 for particles with radii <20 μm.

Rosetta followed comet 67P/Churyumov-Gerasimenko (67P/CG) from 2014 August to 2016 September. It was a unique opportunity for the Visual, Infrared and Thermal Imaging Spectrometer (VIRTIS-M; Coradini et al. 2007), spectral range of 0.25–5 μm, and the Grain Impact Analyser and Dust Accumulator (GIADA; Colangeli et al. 2007; Della Corte et al. 2014) to acquire a relevant amount of dust coma measurements. VIRTIS-M and GIADA provide complementary dust information and combining their measurements provides a powerful means to characterize the dust coma properties. *Rosetta* flew around 67P/CG at speeds ranging 0.5–2 m s^{-1}, i.e. lower than the dust particle radial velocities measured by GIADA, 5–15 m s^{-1}. GIADA data we used to derive the dust size distribution were acquired when pointing the dust detector [with field of view (FOV) < 37°] towards the sunlit nucleus surface. This circumstance excluded any contribution from the dust reflected by the solar radiation pressure and reduces the uncertainties introduced by the unknown ejection anisotropy (Fulle et al. 2016b). This was not the case during previous flybys at other comets, when the phase angles (Sun-comet-spacecraft) were close to 90° and the spacecraft speeds were orders of magnitude larger than the dust velocity.

The aim of this work is to present results of a dust scattering model linking the dust radiance spectra observed by VIRTIS-M to the differential dust size distribution determined by GIADA individual dust particle detections. We present an analysis of the dust data acquired at heliocentric distances of 2 and 1.7 au, a few months before the perihelion passage. The data sets are presented in Section 2; a description of the models and methods adopted is given in Sections 2 and 3. Section 5 describes the results obtained from the analysis. A summary of the main findings is presented in Section 6.

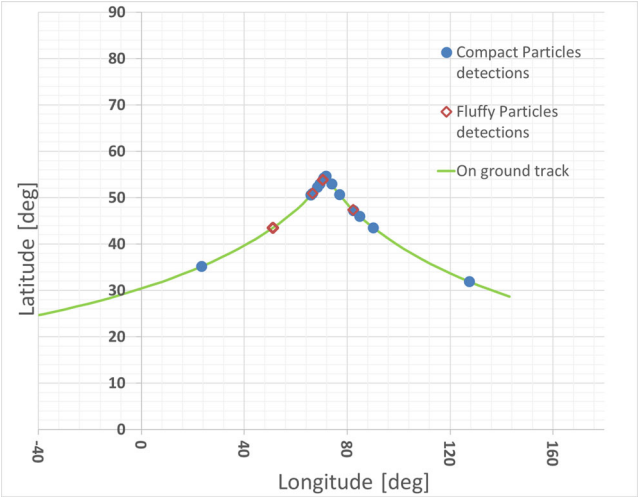


Figure 1. Spatial distribution of the compact and fluffy particles detected by GIADA during the 2015 March 28 flyby. While during the bound-orbit phase the fluffy and compact particle spatial distribution was not correlated, during this flyby the correlation is evident, especially during the closest approach. The continuum green line shows the spacecraft track projected on the comet surface, covering latitude and longitude ranges of 40°–60° N and 30°–90° E, respectively.

2 DATA SET DESCRIPTION

The data used in this work have been acquired by two of the instruments forming part of the *Rosetta* payload, by VIRTIS-M, data acquired on 2015 April 27, and by GIADA, data acquired on 2015 March 28.

VIRTIS is composed of two instruments, a medium-resolution imaging spectrometer (VIRTIS- M) and a high-resolution spectrometer (VIRTIS-H). VIRTIS-M is a long-slit Offner type spectrometer able to acquire hyperspectral images with a maximum spatial resolution of 250 μrad. It has a visible (VIS) section from 0.25 to 1 μm and an infrared (IR) section from 1.0 to 5 μm each sampled by 432 spectral channels. The final result of a VIRTIS-M observation is an image cube, in which two dimensions represent the spatial information (one instantaneous along the slit, samples, and the other obtained by scanning in the direction perpendicular to the slit, lines), while the third dimension is the spectrum (Coradini et al. 2007). Coupled to VIRTIS-M, is a bore-sighted higher resolution pointing echelle spectrometer, VIRTIS-H, with a numerical resolution of about 2000 and a field of view of 500 × 1500 μrad.

GIADA consists of three different detection subsystems assembled in a single instrument with a specific geometry to allow combined measurements. The detections subsystems are (1) the Grain Detection System (GDS), designed to start a time counter when detecting individual dust particle entering GIADA, without affecting its dynamic properties, and to constraint its optical cross-section; (2) the Impact Sensor (IS), a sensitive plate to measure the momentum released by each particles upon impact and (3) the Microbalance System (MBS) to measure the cumulative dust mass coming from five different directions for particle sizes less than 10 μm. On 2015 March 28, *Rosetta* performed a flyby, with a speed of about 1–2 m s^{-1}, at 15 km closest approach distance, covering latitude and longitude ranges of 40°–60° N and 30°–90° E, respectively (Fig. 1). During this flyby, GIADA registered high dust detection rates, thanks to the close distance of *Rosetta* from the nucleus and its passage above high northern latitudes. Before perihelion, northern

Downloaded from https://academic.oup.com/mnras/article/469/Suppl_2/S598/4004761 by guest on 27 April 2021

Table 1. VIRTIS-M observation analysed in this work.

IR file name	Cube dimension[a]	Spatial resolution (px m^{-1})	Start time (h: min: s)	Duration (s)	Distance (km)	Phase angle (○)	Sub/solar latitude (○)	Sub/solar longitude (○)	r_h (au)
I1_00388760487	256 220 432	35	20:25:43	4635	139.57	74.0	2.4	273.87	1.76

Note. [a]Number of samples (256 fixed pixel number), number of scan lines and spectral bands (432 for each channel).

latitudes were in local summer, thus characterized by a high level of dust ejection.

During the whole *Rosetta* scientific phase, GIADA detected two dust particle types: compact and fluffy particles (Fulle et al. 2015; Rotundi et al. 2015). While during the bound-orbit phase the fluffy and compact particle spatial distribution was not correlated (Della Corte et al. 2015), in this case the measurements show a strong correlation and localization of the two particle types (Fig. 1), mostly due to the high detection rate. In Table 1, we show the measurements performed by GIADA on 38 individual particles. Among these, 12 particles were detected in cascade by the GDS and IS subsystems and 26 particles were measured by the IS only. When a dust particle is detected by both the GDS and IS subsystems, its speed is measured and its mass is derived combining the speed and the momentum measurements. In addition, the particle mass and its cross-section, determined by the GDS signal combined with calibration curves (Della Corte et al. 2016a), constrain the particle density (Fulle et al. 2016a). More specifically, a dust particle entering into GIADA crosses the GDS laser curtain that registers a signal proportional to the particle cross-section times the albedo. It also triggers a time counter, which is halted by the impact on the IS. If the optical cross-section of the particle is too small to be detected by the GDS, i.e. radius < 50 μm for dark materials, it is detected by the IS only. In this case, the particle momentum is converted to particle mass assuming the mean, in a certain mass bin, of the speed values measured by the combined GDS and IS detections (Della Corte et al. 2016a), or assuming the velocities predicted by tail models (Fulle et al. 2010).

On 2015 April 27, VIRTIS-M performed observations, when the spacecraft was about 140 km from the comet nucleus with the FOV covering 8.9 km in the horizontal and 7.7 km in the vertical direction. During the data acquisition, the spacecraft was approximately in the terminator orbit so that one half of the nucleus was illuminated and the other half was in shadow. We selected the cube image including the coma region facing the nucleus surface, where GIADA detected the dust particles considered for this work on March 28 (black area in Fig. 2). Fig. 2 shows the comet nucleus as seen by VIRTIS-M (the selected wavelengths are an average between 4.05 and 4.15 μm) superimposed on maps of the dust continuum at 1.1 μm also derived from the VIRTIS-M observation. As a measure of the continuum intensity in the IR, we chose a narrow band pass of 0.1 μm in width, centred at 1.1 μm. The presence of the nucleus in the frame introduces some stray light. The region affected by stray light (the semitransparent blue rectangle shown in Fig. 2) has not been used in this work. The Sun is illuminating the coma from the top of the image. The rotation axis of the comet is along the horizontal direction in the plane of the figure with the spin axis vector tumbling towards the observer. VIRTIS is observing the equator and the line of sight (LOS) passes over both the neck and the illuminated body of the comet. The dust emission has a predictable behaviour correlated with the illumination conditions. The maximum dust intensity, located over the dayside, decreases going from the lit-to-dark side and decreases with distance from the nucleus

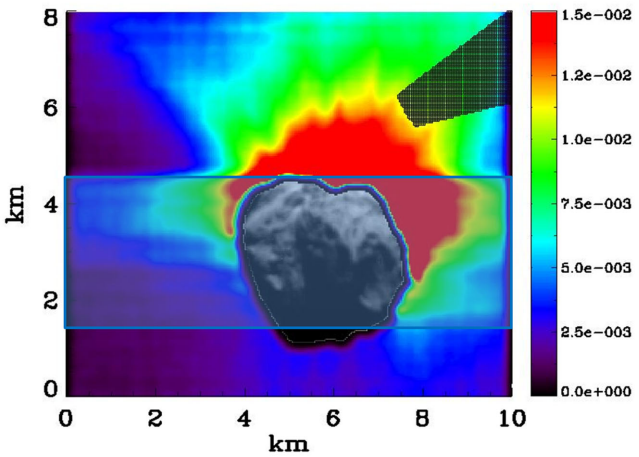


Figure 2. VIRTIS-M data cube (MTP015/STP053/I1_00388787067) acquired on 2015-04-27 at 1.1 μm when the spacecraft was at about 140 km from the nucleus allowing a complete coma coverage at different distances from the surface. A VIRTIS-M image of the nucleus acquired at 4.2 μm is inserted for a better visualization of the data cube. The dust radiance colour bar unit is W m^{-2} sr^{-1} μm^{-1}. The semi-transparent strip indicates the region of the instrumental sensitivity to scattered light from the nucleus. The black area indicates the coma region sampled by GIADA and considered for VIRTIS-M data selection.

(Della Corte et al. 2015, 2016b; Migliorini et al. 2016; Rinaldi et al. 2016).

Although the VIRTIS data cube was acquired 1 month after the GIADA data acquisition, we could combine the two data sets because the 67P/CG dust properties did not change significantly between 2015 March and April (Rinaldi et al. 2016; Bertini et al. 2017). For VIRTIS-M, we consider a mean spectrum obtained inside the black area at the top right of Fig. 2. In Fig. 3, we report the dust coma average radiance spectrum acquired in latitude and longitude ranges where GIADA was measuring on March 28 (black area in Fig. 2). The observed radiance spectrum has been averaged over 2362 pixel. Due to the small size of the black area (about 1.7 $\times$ 2 km), the phase angle can be considered constant for all the dust particles along the VIRTIS LOS, with an average value of 74°. The spectrum shows a continuum, due to light scattered by the dust, which follows the solar radiance fairly closely, and emission bands due to water vapour and CO_2 at 2.7μm and 4.2 μm, respectively. Starting from 3.7 μm, a clear contribution to the radiance from the dust thermal emission is visible. The spectra and images were analysed using the VIRTIS reduction pipeline (Filacchione 2006; Ammannito et al. 2006; Filacchione et al. 2006) and corrections derived from in-flight data (Raponi 2014). The bad pixels or cosmic ray strikes have been removed using a median filter 'de-spiking' algorithm, which is employed only in the horizontal dimension, thus leaving the spectral data intact.

Downloaded from https://academic.oup.com/mnras/article/469/Suppl_2/S598/4004761 by guest on 27 April 2021

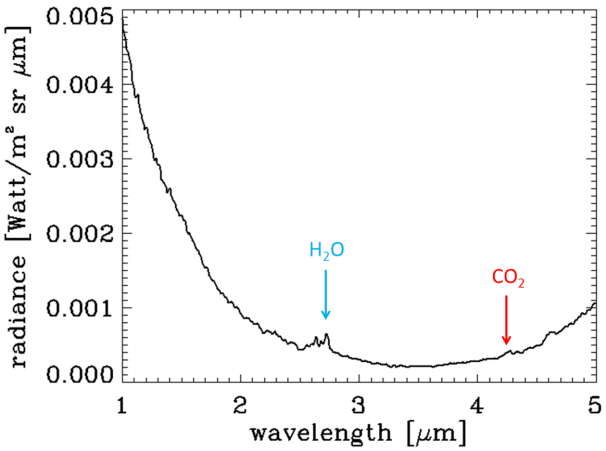


Figure 3. Radiance spectrum acquired on 2015 April 27 for cube I1_00388787067 in the infrared channel averaged inside the black area of the image in Fig. 2. The H_2O and CO_2 emissions at 2.67 μm and 4.27 μm are observed.

In Table 1, we list the parameters for the VIRTIS-M observations in the IR channel. The first column gives file name. The second column lists the image size in number of samples (256 fixed pixel number), number of scan lines and spectral bands (432 for each channel). The third column reports the pixel dimension (m) at the comet distance. The fourth column shows the starting time (UT), while the following column indicates the total time of the observations. In Table 1 are also reported some geometrical parameters such as the subsolar longitude and latitude, which serve as an indicator of the orientation of the comet, the distance from the surface, the phase angle and the heliocentric distance. The geometry information is calculated by an SPICE routine (Acton 1996) using the spacecraft's trajectory/orientation reconstructed kernels and the 67P/CG SHAP5 shape model (Jorda et al. 2016).

3 RADIANCE MODEL

A simple radiative transfer model has been developed to simulate the VIRTIS-M radiances to infer the dust properties. We assumed an optically thin dust coma in local radiative equilibrium and spherical dust particles. The continuum emission detected in VIRTIS-M spectra (I_{obs}) is due to the solar radiation scattered by dust coma (I_{scat}) and due to thermal emission from absorbing particles (I_{therm}) that we describe by a blackbody. For an optically thin coma, the intensity I_{scat} (W m^{-2} sr^{-1} μm^{-1}) scattered by a column of particles of column density $n_{col}n_{col}$ is given by

$$I_{\rm scat} = n_{\rm col}(a) F_s \sigma_{\rm geom} q_{\rm sca}(a, \lambda) \frac{p(g, \lambda)}{4\pi}, \quad (1)$$

where F_s is the incident parallel solar flux (W m^{-2} sr^{-1} μm^{-1}), $\sigma_{\rm geom}$ is the geometric particle cross-section (m^2), a is the particle radius, $q_{\rm sca}(a, \lambda)$ is the scattering efficiency of the dust particles, $p(g, \lambda)$ is the normalized phase function and g is the phase angle. The phase function $p(g, \lambda)$ is normalized such that the integral over the solid angle is 4π. The thermal radiation is approximated by

$$I_{\rm therm} = n_{\rm col}(a) C_T B(\lambda, T_p), \quad (2)$$

where C_T is the absorption cross-section of the particles in the FOV, T_p is the colour temperature and $B(\lambda, T_p)$ is the Plank function. The numerical solutions require the following inputs:

1. An assembled spectrum for the solar flux in the range of 0.25–5 μm. The adopted spectrum is the one assembled by Kurucz using measurements from Kitt Peak, ATMOS Spacelab experiment and theoretical results. These data were taken from LBLRTM 5.21 (http://www.meto.umd.edu/bobe/LBLRTM/). The original Kurucz (1992) data were converted to mWm^{-2} nm^{-1} and averaged over 0.1 nm intervals centred around the given wavelength.
2. A dust model as a function of wavenumber in the range of 1–5 μm (Section 4).

4 DUST MODEL

The dust model basically aims to fix the dust particle shape, size distribution and the (complex) refractive indices. These are the quantities needed to compute the dust contributions to single scattering albedo, single scattering phase function $p(g, \lambda)$ and extinction efficiency.

4.1 Dust particle shape

Comets are time capsules of primitive and irregular dust particles, compact and aggregated, as shown from light scattering studies (Kimura et al. 2016) and from the analysis of Stardust Aluminium foil craters and aerogel penetration tracks (Hörz et al. 2006). GIADA was able to distinguish different types of particles populating the coma of 67P/CG: compact particles and fluffy porous aggregates. The compact particles (Della Corte et al. 2015; Rotundi et al. 2015) have a mean bulk density of 800 kg m^{-3} and a mean porosity of 0.5 (Fulle et al. 2016a). The fluffy particles are porous aggregates of submicron grains ranging in size from 0.2 to 2.5 mm with an equivalent bulk density up to 1 kg m^{-3} (Fulle et al. 2015). Fluffy particle detections normally occurred as showers of numerous particles clustered in space and in time with durations of up to 30 s (Fulle et al. 2015). In this work, in order to model the observed IR radiance spectrum related to an active area (Fig. 2) and associated with the compact particles, we used the Mie scattering theory. This applies to homogeneous spherical grains and provides reliable results in the Rayleigh regime, when the particle size parameter is less than 1.

4.2 Dust composition

During the last 30 years, several cometary flyby missions and laboratory analyses of cometary particles and interplanetary dust particles (IDPs) have provided useful inputs indicating that cometary dust particles are composed of silicates and carbonaceous (CHON) material mixed together on a very fine scale (Jessberger, Christoforidis & Kissel 1988; Rietmeijer 1998; Zolensky et al. 2008). In comet 81P/Wild 2, silicate grains resulted to be much larger than those modelled for interstellar dust. Also many high-temperature minerals, formed in the inner regions of the solar nebula, were observed (Brownlee et al. 2006). In comet 81P/Wild 2 samples, organics are heterogeneously distributed in abundance and composition, in some cases similar to those in IDPs, aromatic-poor organic material are present (Sandford et al. 2006). Cometary dust consists of heterogeneous particles composed by dark material, which determines the low albedo, and minerals, mainly silicates and sulphides (Zolensky et al. 2008; Capaccioni et al. 2015) that are responsible for the spectral features in the thermal infrared spectra. Cometary particle composition can be inferred from the trends in colours and thermal-emission characteristics with the cometocentric distance.

Downloaded from https://academic.oup.com/mnras/article/469/Suppl_2/S598/4004761 by guest on 27 April 2021

Table 2. GIADA detections occurred on 2015 March 28, at Sun-Comet distance of 1.9 au, divided in two sets: (1) particles detected by the GDS and the IS subsystems (N_{GDS+IS}) for which the mass and the speed are measured; (2) particles detected only by the IS subsystems (N_{IS}), for which the momentum is measured and the masses are derived either assuming the dust velocity from Fulle et al. (2010) (indicated by an *), or by considering the average of the speeds measured by GIADA (GDS+IS detections) in a specific momentum bin. In the fourth column, the dust particle speeds (v) are reported. These detections have been acquired at cometocentric distance between 15 and 20 km.

N_{GDS+IS}	N_{IS}	Mass bin (kg)	v (m s^{-1})
0	7	10^{-9}–10^{-8}	15*
5	19	10^{-8}–10^{-7}	9.1
7	0	10^{-7}–10^{-6}	5

Rosetta mission to comet 67P/CG gave us the opportunity to observe coma regions within few km from the surface and to study the dynamical and physical properties of the emitted dust (Rinaldi et al. 2016). This indicates that the dust ejected from the nucleus is quite uniform. The colour of the dust in the coma has a fairly steep red slope in the visible of about 9 to 12 ± 1 per cent per 100 nm, from 0.45 to 0.75 μm, both in the sunlit and dark sides, and a much shallower slope in the IR, from 1 to 2.5 μm, with values of 1.7 ± 0.2 per cent per 100 nm in the sunlit and 3 ± 1 per cent per 100 nm on the dark side. As shown in Fig. 3, there are no evident absorption features in the IR spectrum, so for the dust model we can adopt a featureless material to reproduce the reddening characteristics in the model. This is supported by the GIADA (Della Corte et al. 2016a) calibration curve selection used for GIADA/GDS data analysis: the curve using as cometary analogue (Ferrari et al. 2014) amorphous carbon particles is the only one applicable to evaluate the particle geometrical cross-section. In fact, applying calibration curves obtained for brighter material lead to unrealistic particle densities. To model the observed radiance spectra, we used the amorphous carbon optical constants derived by Colangeli et al. (1997).

4.3 Differential particle size distribution

Coupling the 38 particle mass measurements performed by GIADA (Table 2) on 2015 March 28 and 74 particles imaged by OSIRIS on 2015 March 14, published by Fulle et al. (2016b) and listed in Table 3, we derive the dust size distribution over eight mass bins, from 10^{-10} to 10^{-2} kg (Fig. 4). The dust size distribution at the sunlit nucleus surface is derived by fitting the dust volume density (n_{vol}) as a function of the dust particle sizes. The volume density for a simple analytical dust outflow model is

$$n_{vol}(r) = \frac{Q_n}{2\pi v_d r^2}, \quad (3)$$

where r is the radial distance from the nucleus centre (4 km), Q_n is the equivalent spherical dust production rate at the nucleus and v_d is the measured dust radial velocity (Table 4). The radius bin size has been calculated from the mass bin and an average dust particle bulk density (ρ) of 800 kg m^{-3} (Fulle et al. 2016a). Fig. 4 shows the measured dust size distribution as a function of eight size bin on logarithmic scale. We fitted the size distribution with a power law deriving an index of −2.2 ± 0.3 (red line in Fig. 4).

Table 3. Particles size and fluxes measured by GIADA and OSIRIS on 2015 March 28 and 14, respectively. The OSIRIS data are taken from Fulle et al. (2016b, table 6). Particle masses and sizes are calculated assuming a dust bulk density of 10^3 kg m^{-3} (Fulle et al. 2016b). Q_n is the dust number loss rates at the nucleus surface, v is the measured dust radial velocity and r_h is the heliocentric distance. For the mass bin, 10^{-6}–10^{-5} kg, GIADA did not detect any particles, thus we considered the Q_n and v values by Fulle et al. (2010).

Instrument	Mass (kg)	Size (m)	Q_n (♯ s^{-1})	v (m s^{-1})	R_h (au)
GIADA	5×10^{-9}	8.42×10^{-5}	1.1×10^7	15	2.0
GIADA	5×10^{-8}	0.00018	1.1×10^8	9.1	2.0
GIADA	5×10^{-7}	0.00039	5×10^8	5	2.0
GIADA	5×10^{-6}	0.00084	1.1×10^7	2.2	2.0
OSIRIS	5×10^{-5}	0.00181	3.1×10^5	1.9	1.9
OSIRIS	5×10^{-4}	0.00390	8×10^3	1.7	1.9
OSIRIS	5×10^{-3}	0.00841	1.8×10^3	1.6	1.9
OSIRIS	5×10^{-2}	0.01813	20	2.7	1.9

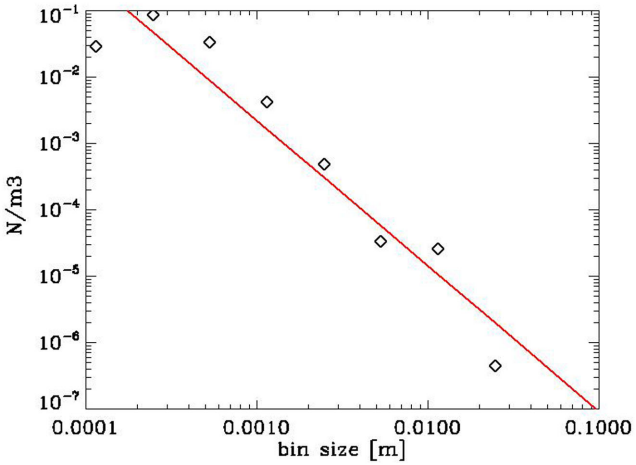


Figure 4. Dust volume density derived by GIADA measurements (this work) and by OSIRIS data (Fulle et al. 2016b) as a function of the dust particles bin size. The red line is the best fit providing a slope of −2.2 ± 0.3.

5 FITTING RESULTS

We fitted the observed spectrum (Fig. 3) with our radiance model using a range of power-law size distribution indexes. This approach allowed us to verify the sensitivity of the VIRTIS measured radiance to the variation of the index and the size range of the differential dust size distribution. In addition, we could directly compare the remote sensing observations to the *in situ* GIADA measurements. We used dust size distributions with power-law indexes from −4 to −0.1, particle size intervals between 0.1 and 1000 μm and a linear least square fitting algorithm to invert the observed spectra. The dust physical parameters are iteratively varied by means of a minimization algorithm until the best fit is achieved. The optimization is performed only in the dust continuum range, excluding the vapour emission bands of H_2O and CO_2, at 2.7 μm and 4.2 μm, respectively. In Fig. 5, the minimum residual (between the observed spectrum and its best fit) versus the power index is plotted. The higher residuals for indexes <-3.1 demonstrate inconsistency between modelled spectra and observations (Fig. 6). For indexes >-3.1, we find almost constant minimum residuals meaning that the IR spectra can be fitted with any differential size distribution dominated by larger grain sizes, which is in agreement with

Downloaded from https://academic.oup.com/mnras/article/469/Suppl_2/S598/4004761 by guest on 27 April 2021

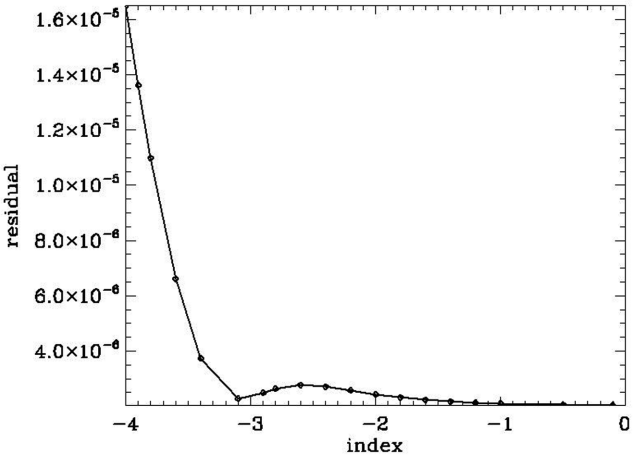


Figure 5. The minimum residual between the observed spectrum and its best fit versus the power-law index. The higher residuals correspond to indexes <-3.1. For indexes >-3.1, the plot shows almost constant minimum residuals, meaning that the IR spectra can be fitted with any differential size distribution dominated by larger grain sizes, which is in agreement with findings by Crifo (1987).

findings of Crifo (1987). The residual plot (Fig. 5) suggests that the differential size distribution index is $-3.1^{+3}_{-0.1}$

This power index, best fitting the VIRTIS-M spectrum acquired in the same coma region sampled by GIADA, is consistent with the dust size distribution power-law indexes retrieved combining GIADA (section 4.3) and OSIRIS data (Fulle et al. 2016b). In Fig. 6, we compare the observed radiance spectrum (black curve) and the best-fitting model at VIRTIS-M spectral resolution of 0.1 μm (red curve). The synthetic spectrum is computed using a size distribution with an index power law of −4, −3.1 and −2.2. The dust continuum is fitted only for size distribution power laws of −3.1 and −2.2. The only mismatch between the observed spectrum and the fit is found in the 3.0–3.7 μm range, suggesting the presence of the organic band in 67P/CG dust, already detected in the 67P/CG nucleus (Capaccioni et al. 2015) as well as in 81P/Wild2 dust particles and in the Galactic Centre Source SGRA (Rotundi & Rietmeijer 2008).

The ratios (in per cent) of the computed radiance for two particle size ranges split at 10 μm grain size and normalized by the total radiance for power-law index of −4, −3.1, −2.2 are shown in Fig. 7. We chose 10 μm as boundary size limit to define the range for small and large particles with respect to IR wavelengths.

The reported plots show that a power-law index of −4 corresponds to a major contribution to the IR radiance coming from small particles, while with a power-law index of −2.2 large particles dominate. For a power index of −3.1, the contribution of small and large particles is comparable. The VIRTIS-M spectrum best fit is obtained with all power-law indexes >-3.1.

We retrieved the column particle number densities and the colour temperature. Gehrz and Ney (1992) define the superheat parameter $S = T_p/T_{BB}$ as the ratio of the observed dust coma temperature (T_p) and the perfectly conducting black sphere expected temperature ($T_{BB} = 278/\mathrm{rh}^{0.5}$), at the same heliocentric distance. We derived $T_p = (210 \pm 11)$ K by fitting the thermal part of the spectrum that gives a superheat value of $S = 1.0 \pm 0.05$ for all indexes greater than −3.1. This superheat value confirms that the 67P/CG dust particles, at the time of GIADA and VIRTIS observations, were relatively large (Gehrz & Ney 1992). The retrieved column number densities

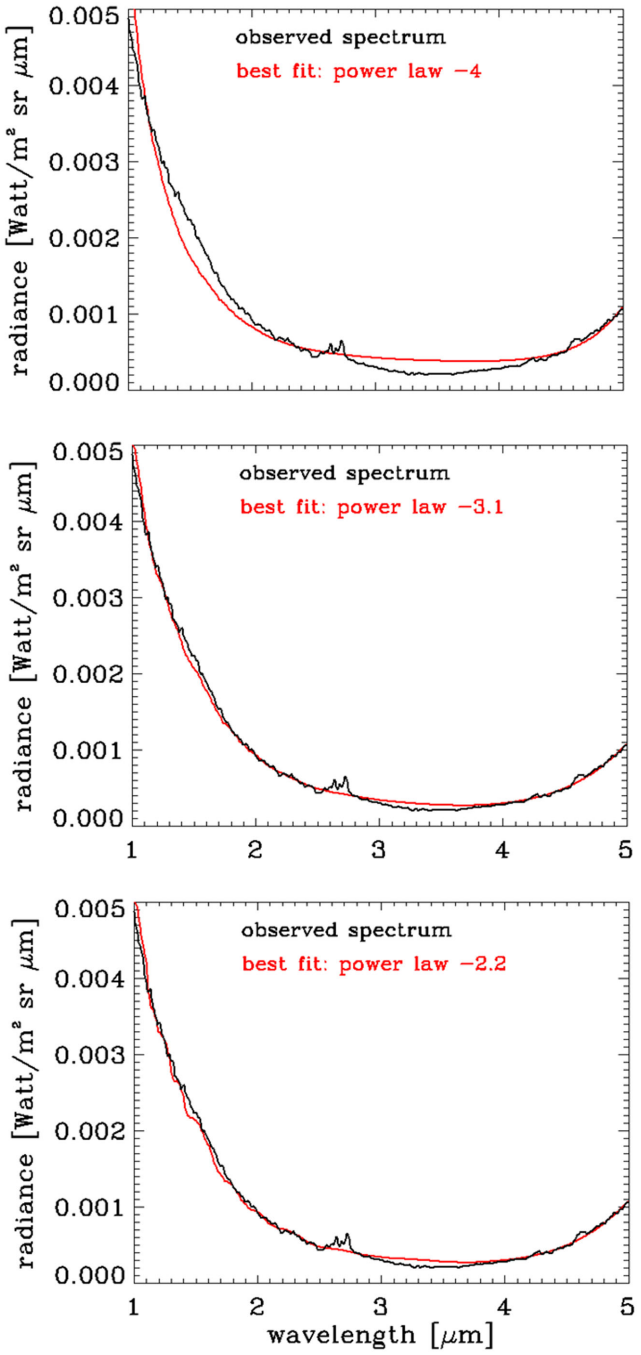


Figure 6. The observed radiance spectrum acquired on 2015 April 27 in the infrared channel (black curve) and the best fit (red curve) computed with power-law indexes of −4.0, −3.1 and −2.2. The spectrum is well reproduced with power-law indexes of −3.1 and −2.2 with the exception of the range 3.0–3.8 μm, probably due to the presence of organics in the dust particles.

range between 1.6×10^{11} and 36 ♯ m^{-2}, with an error of 10 per cent, for power-law indexes between −3.1 and −0.1.

6 CONCLUSIONS

The *Rosetta* mission to comet 67P/CG gave us the opportunity to observe the regions of the coma within a few km from the nucleus surface and to investigate the physical properties of the ejected

Downloaded from https://academic.oup.com/mnras/article/469/Suppl_2/S598/4004761 by guest on 27 April 2021

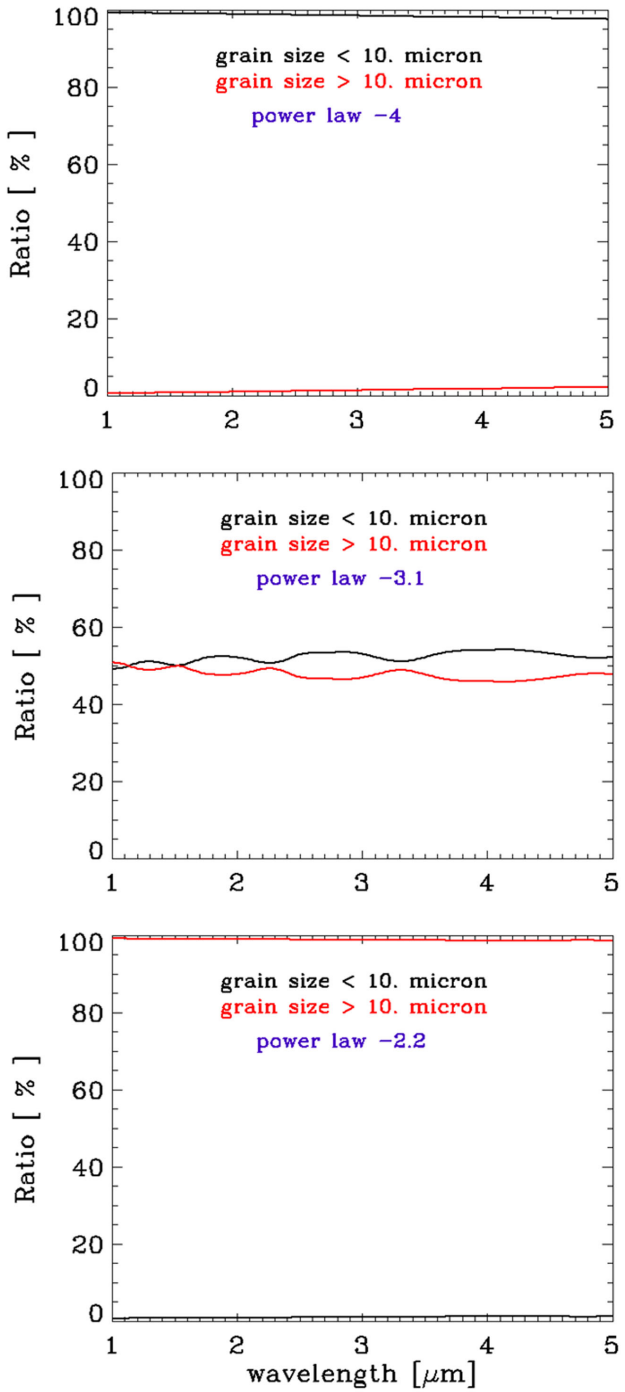


Figure 7. Ratios (in per cent) of the computed radiance, normalized by the total radiance, calculated for power-law indexes of −4.0, −3.1 and −2.2 for two different grain size ranges: small particles of 0.1–10.0 μm and large particles of 10 μm −1 mm. The major contribution to the IR radiance comes from small particles in the case of power index −4.0 and large particles in the case of power −2.2. For a power index of −3.1, the contribution of small and large particles is comparable.

dust. Combining VIRTIS-M and GIADA observations, we determined the differential size distribution and characterized the physical properties of the dust present in the coma. Our main results can be summarized as follows:

(1) The coma dust continuum radiation, observed by VIRTIS-M, is sensitive to the dust size distribution. A power-law index of −4 fails in reproducing the observation. All synthetic spectra computed by means of a differential size distribution with power-law index greater than −3.1 match the dust continuum very well.

(2) The GIADA dust size distribution power-law indexes, here retrieved, are consistent with those best fitting the VIRTIS-M spectrum acquired in the same coma region sampled by GIADA.

(3) Before perihelion, the dust ejected into the inner coma from the nucleus does not change its spectral properties and size distribution from 2015 March to April, confirming Rinaldi et al. (2016) results.

(4) Before perihelion, the inner coma radiance is dominated by particles greater than 10 μm.

(5) The only mismatch between the observed and synthetic spectra occurs in the range of 3.0–3.7 μm, suggesting the presence of organics in the dust particles. Work is in progress for a focused paper on this critical subject.

ACKNOWLEDGEMENTS

The authors would like to thank the following institutions and agencies that supported this work: Italian Space Agency (ASI – Italy), Centre National d'Etudes Spatiales (CNES- France), Deutsches Zentrum für Luft- und Raumfahrt (DLR-Germany), National Aeronautic and Space Administration (NASA-USA) *Rosetta* programme, and Science and Technology Facilities Council (UK). VIRTIS has been built by a consortium, which includes Italy, France and Germany, under the scientific responsibility of the Istituto di Astrofisica e Planetologia Spaziali of INAF, Italy, which guides also the scientific operations. The VIRTIS instrument development has been funded and managed by ASI, with contributions from Observatoire de Meudon financed by CNES, and from DLR. The authors wish to thank the *Rosetta* Science Ground Segment and the *Rosetta* Mission Operations Centre for their dedication and support throughout the phases of the mission.

GIADA was built by a consortium led by the Universita' degli Studi di Napoli Parthenope and INAF – Osservatorio Astronomico di Capodimonte, in collaboration with the Institutode Astrofisicade Andalucia, Selex-ES, FI, and SENER. GIADA is presently managed and operated by Istituto di Astrofisica e Planetologia Spaziali – INAF, Italy. GIADA was funded and managed by the Agenzia Spaziale Italiana (contract number I/024/12/1), with the support of the Spanish Ministry of Education and Science Ministerio de Educaciony Ciencias (MEC). GIADA was developed from a Principal Investigator proposal from the University of Kent; science and technology contributions were provided by CISAS, Italy; Laboratoire d'Astrophysique Spatiale, France; and institutions from the United Kingdom, Italy, France, Germany and the United States.

REFERENCES

Acton C. H., 1996, Planet. Space Sci., 44, 65
Ammannito E., Filacchione G., Coradini A., Capaccioni F., Piccioni G., de Sanctis M. C., Dami M., Barbis A., 2006, Rev. Sci. Instrum., 77, 093109
Bertini I. et al., 2017, MNRAS, in this issue
Brownlee D. et al., 2006, Science, 314, 1711
Capaccioni F. et al., 2015, Science, 347, aaa0628
Colangeli L., Bussoletti E., Pestellini C. C., Mennella V., Palomba E., Palumbo P., Rotundi A., 1997, Adv. Space Res., 20, 1617
Colangeli L. et al., 2007, Space Sci. Rev., 128, 803
Coradini A. et al., 2007, Space Sci. Rev., 128, 529

Downloaded from https://academic.oup.com/mnras/article/469/Suppl_2/S598/4004761 by guest on 27 April 2021

Crifo J. F., 1987, in Rolfe E. J., Battrick B., eds, ESA SP-278: Diversity and Similarity of Comets
Della Corte V. et al., 2014, J. Astron. Instrum., 3, 1350011
Della Corte V. et al., 2015, A&A, 583, A13
Della Corte V. et al., 2016a, Acta Astronautica, 126, 205
Della Corte V. et al., 2016b, MNRAS, 462, S210
Ferrari M., Della Corte V., Rotundi A., Rietmeijer F. J. M., 2014, Planet. Space Sci., 101, 53
Filacchione G., 2006, Calibrazioni a terra e prestazioni in volo di spettrometri ad immagine nel visibile e nel vicino infrarosso per l esplorazione planetaria. PhD dissertation, Universita degli Studi di Napoli Federico II.
Filacchione G., Ammannito E., Coradini A., Capaccioni F., Piccioni G., de Sanctis M. C., Dami M., Barbis A., 2006, Rev. Sci. Instrum., 77, 103106
Fulle M., Colangeli L., Mennella V., Rotundi A., Bussoletti E., 1995, A&A, 304, 622
Fulle M., Levasseur-Regourd A. C., McBride N., Hadamcik E., 2000, AJ, 119, 1968
Fulle M. et al., 2010, A&A, 522, A63
Fulle M. et al., 2015, ApJ, 802, L12
Fulle M. et al., 2016a, MNRAS, 462, S132
Fulle M. et al., 2016b, ApJ, 821, 19
Gehrz R. D., Ney E. P., 1992, Icarus, 100, 162
Green S. F. et al., 2007, Dust Planet. Syst., 643, 35
Hörz F. et al., 2006, Science, 314, 1716
Jessberger E. K., Christoforidis A., Kissel J., 1988, Nature, 332, 691
Jorda L. et al., 2007, Icarus, 187, 208
Jorda L. et al., 2016, Icarus, 277, 257
Kimura H., Kolokolova L., Li A., Lebreton J., 2016, preprint (arXiv:1603.03123)
Kurucz R. L., 1992, in Rabin D. M., Jefferies J. T., eds, Proc. IAU Symp. 154, Synthetic Infrared Spectra in Infrared Solar Physics. Kluwer Acad. Press, Norwell, MA
Lisse C. M. et al., 2006, Science, 313, 635
Lisse C. M. et al., 2007, Icarus, 190, 391
McDonnell J. A. M. et al., 1987, A&A, 187, 719
Migliorini A. et al., 2016, A&A, 589, A45
Raponi A., 2014, Spectrophotometric analysis of cometary nuclei from in situ observations. PhD dissertation, Universitá degli studi di Roma Tor Vergata
Rietmeijer F. J. M., 1998, Interplanetary Dust Particles. p. 2
Rinaldi G. et al., 2016, MNRAS, 462, S547
Rotundi A., Rietmeijer F. J. M., 2008, Earth Moon Planets, 102, 473
Rotundi A. et al., 2015, Science, 347, aaa3905
Sandford S. A. et al., 2006, Science, 314, 1720
Zolensky M. et al., 2008, Meteorit. Planet. Sci., 43, 261

This paper has been typeset from a TEX/LATEX file prepared by the author.

Downloaded from https://academic.oup.com/mnras/article/469/Suppl_2/S598/4004761 by guest on 27 April 2021